Available online at www.sciencedirect.com
SCIENCE DIRECT®
Journal of Magnetic Resonance 180 (2006) 311–317
JMR Journal of Magnetic Resonance
www.elsevier.com/locate/jmr

Communication

Resolution enhancement in 1D solid-state NMR spectra of spin-9/2 quadrupolar nuclei

Jean-Paul Amoureux *, Julien Trébosc

UCCS, CNRS-8181, University of Lille-1, C7-ENSCL, 59652 Villeneuve d'Ascq, France

Received 17 January 2006; revised 27 February 2006
Available online 22 March 2006

Abstract

NMR is an insensitive spectroscopy, which often requires numerous accumulations, especially for 2D high-resolution methods (MQMAS and STMAS) for quadrupolar nuclei in solids. This may be a very important limitation for the case of insensitive nuclei, where a 1D spectrum with better resolution than the central-transition is then highly desirable. This problem has been addressed for the case of spin-5/2 nuclei by the Double-Quantum Filtered Satellite Transition Spectroscopy: DQF-SATRAS-ST_1. We extend this concept to the spin-9/2 nuclei with the SATRAS-ST_2 method. This method allows the observation of 1D spectra with a much better resolution than that observed in the isotropic projection of 2D MQ/ST_1-MAS spectra. This enhanced resolution results from the much smaller homogeneous broadening that occurs on the SATRAS-ST_2 method as compared to MQ/ST_1-MAS spectra. The main interest in this method is for well-crystallized samples.

Keywords: Magic-angle spinning NMR; Quadrupolar nuclei; Satellite-transition MAS; High-resolution; Homogeneous broadening

Nuclear magnetic resonance (NMR) is one of the most powerful tools available to the community of researchers in various areas of physics, chemistry, materials science, biology, and medicine. The ability of NMR to probe the structure of materials strongly depends upon the availability of high-resolution spectra, which serve as fingerprints of the physico-chemical surroundings of the studied nuclei. Initially, such spectra could only be obtained in liquids. In static powders, the nuclear spins experience various anisotropic interactions, which broaden their spectra and render NMR more difficult for structural determination. For spin-1/2 nuclei these interactions include dipole–dipole coupling between spins, chemical shift anisotropy (CSA), indirect spin–spin coupling and any interaction with unpaired electrons. The resolution and sensitivity gap between liquid and solid-state NMR began to decrease in the 1960's with the introduction of radio frequency (RF) decoupling, and magic angle spinning (MAS) [1].

Until recently, however, these techniques could not overcome the line broadening in NMR spectra of the quadrupolar nuclei: with spin greater than 1/2. This broadening arises from the coupling of the non-spherical charge distribution of such nuclei with the gradients of the electric field created by the surrounding electrons. The quadrupolar broadening is 'more anisotropic' than the 1st-order interactions (CSA and dipolar couplings), in the sense that it contains 2nd-order orientational terms of significant magnitude. Therefore, NMR of half-integer spin-quadrupolar nuclei ($S = 3/2$, 5/2, 7/2, 9/2) was limited for a long period of time to the observation of one-dimensional (1D) MAS spectra. These spectra are not of high-resolution, as they remain broadened by the 2nd-order quadrupolar interaction. Complete spatial averaging requires either mechanical rotation around two axes, as in double rotation (DOR) [2], or correlation of signals acquired at two different angles in a two-dimensional (2D) experiment, as in dynamic angle spinning (DAS) [3]. However, both experiments have many technical shortcomings. The observation of quadrupolar nuclei with half-integer spin got a

* Corresponding author. Fax: +33 3 20 43 68 14.
E-mail address: jean-paul.amoureux@univ-lille1.fr (J.-P. Amoureux).

1090-7807/$ - see front matter © 2006 Elsevier Inc. All rights reserved.
doi:10.1016/j.jmr.2006.02.018

significant boost in 1995, with the introduction of the 2D multiple-quantum MAS (MQMAS) method that correlates a multiple-quantum coherence during the evolution time t_1 with the central-transition (CT) during the observation time t_2 [4]. A complementary technique was proposed in 2000 with the introduction of the 2D satellite-transition MAS (STMAS) method, which correlates the satellite transitions (ST) during t_1 with the CT during t_2 [5]. For all crystallite orientations, both methods refocus the 2nd-order quadrupole dephasings along a unique axis ($t_{2e} = Rt_1$), thus leading to observation of high-resolution 2D spectra.

However, NMR is an insensitive spectroscopy, which often requires numerous accumulations, especially for 2D high-resolution methods for quadrupolar nuclei in solids. This may be a very important limitation for the case of insensitive nuclei, those either with a small gyromagnetic ratio, low natural abundance, long relaxation time, or with nuclei that are subject to strong quadrupole interactions. In these cases, a 1D spectrum with better resolution than the CT MAS spectrum is highly desirable. This problem has been very recently addressed for spin-5/2 nuclei by the Double-Quantum Filtered Satellite Transition Spectroscopy: DQF-SATRAS-ST_1 [6]. In this method, after initial excitation with a strong RF pulse, the inner-satellite (ST_1: $1/2 \leftrightarrow 3/2$, $-3/2 \leftrightarrow -1/2$) coherences are filtered from the other satellite transitions by two CT-selective soft π pulses. The signal is then recorded with rotor-synchronized acquisition to fold in all sidebands stemming from 1st-order quadrupole interactions. It is well known that for spin-5/2 nuclei in MAS, the 2nd-order ST_1 quadrupole frequency spread and induced-shift are decreased by the factor 24/7 and 8, respectively, with respect to those observed for the CT [7]. This DQF-SATRAS-ST_1 1D method thus leads to enhanced resolution with respect to MAS, especially for well-crystallized samples, or nuclei mainly subject to quadrupolar distributed parameters [6].

In this communication, we would like to extend this concept to the spin-9/2 nuclei with the SATRAS-ST_2 method. Indeed, it is well known that the second satellite transitions (ST_2: $3/2 \leftrightarrow 5/2$, $-5/2 \leftrightarrow -3/2$) of spin-9/2 nuclei present in MAS an even more favorable scaling of the 2nd-order quadrupolar frequency spread: only 1/18th that of the CT [7].

The corresponding pulse sequence is shown in Fig. 1. It consists of one strong hard-pulse immediately followed by a single CT-selective soft π pulse. The acquisition is made in a rotor-synchronized way, to avoid 1st order quadrupole interactions and to add-up all ST_2 signals. The first pulse must be optimized to create the maximum ST_2 coherences, and its phase cycling only selects the $-1Q$ level. In the framework of a perfectly selective on-resonance irradiation, the CT-selective soft π pulse: (i) inverts the CT magnetization to the $+1Q$ level, (ii) transfers the ST_1 magnetization to the $-2Q$ level and (iii) does not affect the ST_2, ST_3, and ST_4 coherences [8], which thus remain observable. Happily, signals related to ST_3 and ST_4 coherences have much smaller amplitudes than that of ST_2 due

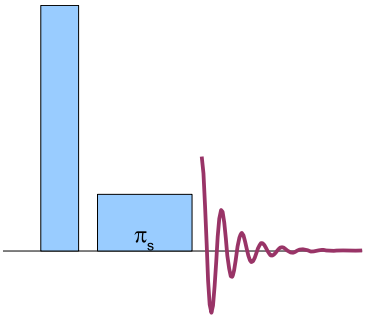

Fig. 1. Pulse-sequence for the SATRAS-ST_2 method. Mathematically, the first pulse should be cycled with at least 11 phases to select only the $-1Q$ level. However, due to the weak RF field of the selective π pulse, 3 or 4 phases are in most cases sufficient for the first pulse. In that case, and also to avoid any phase-transient effects related to the short hard-pulse, a cycling of the CT-selective π pulse, with at least three phases, can be used.

to their weaker intensities and much broader 2nd-order quadrupolar line-widths. Indeed, after an ideal π/2 hard-pulse, the intensities for the CT and the ensembles of the two symmetrical ST_1, ST_2, ST_3, and ST_4 coherences are equal to 25/165, 48/165, 42/165, 32/165, and 18/165, respectively. In practice, the relative intensity of ST_2 is increased with respect to these values by optimizing the first hard-pulse length. This optimization can be done directly on the FID by maximizing the amplitude of one of the ST rotational resonances observed after several (10–20) rotor periods. Indeed, for long acquisition time, these rotational resonances are mainly composed of ST_2 signals, due to their much smaller 2nd-order quadrupolar line-widths. It can also be performed on the SATRAS-ST_2 spectrum. Large $C_Q = e^2qQ$ values are often encountered for spin-9/2 nuclei: $C_Q = 20$ MHz is a typical value for niobium nuclei [9,10]. Therefore, the total frequency spread of all ensembles of the two symmetrical ST_n coherences, which is equal to $nC_Q/12$, often extends over several MHz. As a result, due to the limited probe band-with (FWHM ≈ 1–2 MHz), a larger part of the signal is filtered out for ST_3 and ST_4 coherences than for ST_2 ones. By using density matrix calculations, with $\nu_o = 97.9$ MHz, RF = 200 kHz, 0.8 μs, $C_Q = 20$ MHz, $\eta_Q = 0$, and a probe band-width equal to 2 MHz (FWHM), we have found that the integrated intensities of the external STs then remain smaller than 34% (ST_3) or 9% (ST_4) that of ST_2. Moreover, the total 2nd-order frequency spread of the coherences is equal to 1, 55/72, 1/18, −9/8, and −25/9 in units of $(1 + \eta_Q/6)^2 C_Q^2/336\nu_o$, for CT, ST_1, ST_2, ST_3, and ST_4 coherences, respectively [7]. A negative sign implies a reverse line-shape with respect to that of the CT. Globally, taking into account the respective integrated intensities and 2nd-order line-widths of the satellite transitions, the experimental amplitudes of the outer STs then remain smaller than ca. 2% (ST_3) and 0.2% (ST_4) that of ST_2, and are thus hardly observable on the spectra. In addition, it must be noted that these weak ST_3 and ST_4 resonances are well separated from the other signals, as the quadrupole-induced shifts of the various coherences are equal to

1, 5/8, −1/2, −19/8, and −5 in units of $-(1+\eta_Q^2/3)C_Q^2/720\nu_o$, for CT, ST_1, ST_2, ST_3, and ST_4, respectively. However, a good elimination of CT and ST_1 coherences requires a perfectly CT-selective soft π pulse, which is hard to obtain due to the dispersion of 2nd-order quadrupole interaction and off resonance irradiation related to CSA or differences of chemical and quadrupole-induced shifts. In such difficult cases, it has been shown that the remaining CT signal can also be eliminated by data processing of the FID, especially for medium or large C_Q values [11]. Creation of a large ST_2 signal, requires the use of a strong RF hard-pulse in order to best excite a maximum signal in crystallites with large ST_2 offset frequencies. By using density matrix calculations, we have found that for $C_Q = 20$ MHz and $\eta_Q = 0$, the ST_2 signal is enhanced by a factor 3.5 when doubling the RF amplitude from 100 to 200 kHz. We have also observed that the optimum hard-pulse length is only slightly dependent on the RF field.

As a first test sample, we have used $LiNbO_3$, which presents a single niobium species [12] with quadrupole parameters: $C_Q = 22.1$ MHz, and $\eta_Q = 0$ [13]. Fig. 2 presents two hard-pulse MAS spectra with (Fig. 2a) and without (Fig. 2d) rotor-synchronized acquisition, so that the DQF-SATRAS-ST_1 (Fig. 2c) and SATRAS-ST_2 (Fig. 2b) spectra. The four experiments have been performed with an RF field of 200 kHz, and the same number of accumulated scans. In Fig. 2d, the ST_2 center-band (Fig. 2b) is visible at 35 ppm, but not the other ST center-bands due to their breadth. With rotor-synchronized acquisition all ST sidebands are aliased onto their center-bands (Fig. 2a), which are thus greatly enhanced. The resonance between 0 and −200 ppm is then changed with respect to that in Fig. 2d, due to the large increase of the ST_1 resonance (Fig. 2c), which partly overlaps with that of the CT. In Figs. 3a and b, are represented two SATRAS-ST_2 spectra, and the isotropic projection of a 3QMAS spectrum (Fig. 3c). Experimentally, with the RF amplitudes assumed previously in the simulations (100 and 200 kHz), we have observed exactly the same signal enhancement of 3.5, as can be observed in Figs. 3a and b. As the ^{93}Nb chemical shift range is very large [10], it is important to use a fast spinning speed to avoid folding of the resonances for the various species. This requires a small rotor diameter, which also helps to obtain large RF amplitudes to increase the S/N ratio despite smaller volume. Figs. 3a and b, shows that all other coherences do not appear on the spectra. Indeed, due to the quadrupole-induced shifts, the gravity centers of these resonances should be located at −71 (Fig. 2d), −44 (Fig. 2c), 35 (Fig. 2b), 168, and 355 ppm, from the actual chemical shift, for the CT, ST_1, ST_2, ST_3, and ST_4 coherences, respectively. Moreover all resonances, except ST_2, experience line-widths on the order of the spectral-width and thus any remaining intensity is lost in the base line. It must be noted, that in this case, we have not used any data treatment to eliminate the CT resonance. Fig. 3c displays the isotropic projection of a sheared 3QMAS z-filter [14] spectrum in unified ppm scaling [15,16]. The center of gravity of this spectrum is close to that of the SATRAS-ST_2 spectra, as their quadrupole-induced shifts have close values of +42, and +35 ppm for 3QMAS and SATRAS-ST_2, respectively, on a 9.4 T spectrometer. From the quadrupole parameters, the *total* 2nd-order quadrupole frequency spread is equal to 152 ppm for the CT (Fig. 2d), and hence should be of 8.4 ppm for ST_2. Actually,

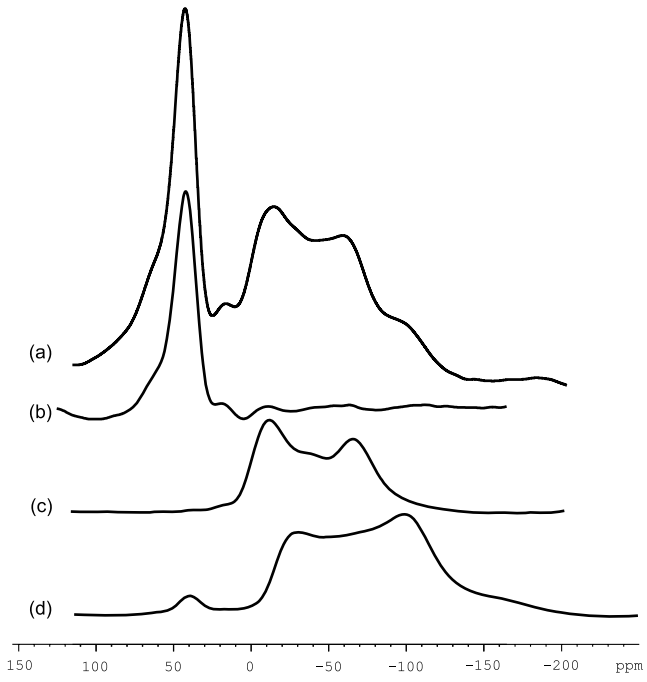

Fig. 2. ^{93}Nb MAS spectra of $LiNbO_3$ recorded at 9.4 T with same number of accumulated scans (8192), acquired using a 2.5 mm probe, and referenced with respect to the chemical shift of this compound. $\nu_o = 97.8$ MHz, $\nu_R = 31250$ Hz, RF = 200 kHz and 5 kHz for the hard and soft pulses, respectively. (a) MAS spectrum with rotor-synchronized acquisition. (b) SATRAS-ST_2 and (c) DQF-SATRAS-ST_1 spectra. (d) Regular MAS spectrum.

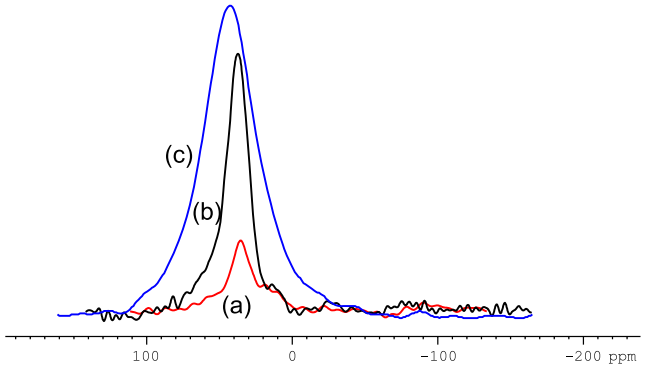

Fig. 3. ^{93}Nb spectra of $LiNbO_3$ recorded at 9.4 T and referenced with respect to the chemical shift of this compound. RF = 5 kHz for soft pulses, recycling delay: 1 s. SATRAS-ST_2 spectra with: (a) RF = 100 kHz, $\nu_R = 24$ kHz, and (b) RF = 200 kHz, $\nu_R = 33$ kHz. Both experiments were acquired in 4 min, using a 2.5 mm probe with 256 scans. (c) Isotropic projection of a 3QMAS spectrum, acquired in 48 min on a 4 mm probe with $\nu_R = 14$ kHz, RF = 150 kHz.

the ST_2 *total* 2nd-order frequency spread is much larger: ca. 70 ppm, (Fig. 3b). This increased broadening may have two origins: a distribution of surroundings due to vacancies [17], which can also be observed on the right-side of Fig. 2d, or a homogeneous broadening.

In a second step, we have analyzed the ^{93}Nb SATRAS-ST_2 spectra of a second sample, namely $Na_4Nb_8P_4O_{32}$, on a 18.8 T spectrometer. From the structure analysis [18], this sample has a P_{1211} monoclinic space-group and thus possesses four inequivalent niobium species, which can be separated into two groups of two similar species. The MAS spectrum is broad, and has been acquired with a CT-selective echo-type experiment. In spite of the fast spinning speed, $\nu_R = 33.333$ kHz, two sidebands due to CSA [10] are observable in the spectrum, and the two overlapping groups of resonances are only slightly discernible onto the center-band (Fig. 4a). The sheared 2D SPAM-3QMAS [19] spectrum presented in Fig. 4b, resolves the two groups, but not the four individual species. It must be noted that: (i) its projection along the direct dimension (Fig. 4c) is better resolved that the 1D MAS spectrum (Fig. 4a), but that its isotropic projection only partly resolves the two groups (Fig. 4d). On the contrary, the two groups are perfectly resolved on the SATRAS-ST_2 spectrum (Fig. 4e). We observe that the integrated intensities of these two groups are approximately equal, as predicted by the structure determination. However, one must be aware that because

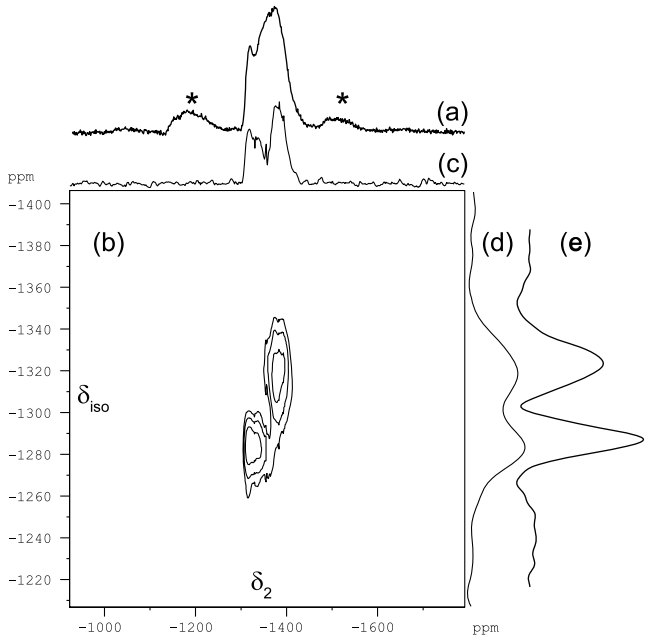

Fig. 4. ^{93}Nb spectra of $Na_4Nb_8P_4O_{32}$ recorded at 18.8 T and referenced to $NbCl_5$ in acetonitrile. $\nu_o = 195.6$ MHz, $\nu_R = 33333$ Hz, RF = 130 and 8 kHz (90°s = 6.25 μs) for hard and CT-selective soft pulses, respectively. Recycling delay: 500 ms. (a) 1D echo MAS CT-selective spectrum: 90°s − τ − 180°s − τ (τ = 30 μs), *indicates sidebands. (b) 2D SPAM-3QMAS spectrum using 1200 scans, 21 echoes, and 4 anti-echoes, with a total experimental time of 250 min, (c) 1D MAS projection of (b). (d) 1D isotropic projection of (b). (e) 1D SATRAS-ST_2 spectrum acquired with 512 scans in 4 min.

of the limited probe bandwidth compared to the total width ($C_Q/6$) of the ST_2 satellites, and different sequence sensitivity relative to the quadrupole interaction, the 2nd-order line-shapes and relative intensities may be distorted in case of multi-site samples with different quadrupole interactions. Simultaneously, it must also be remembered that the same problem of line-shape distortion and non-quantitativity of relative intensities also occurs with MQMAS and STMAS. If we define the resolution as the ratio between the separation of the resonances and their line-widths, the SATRAS-ST_2 spectrum is better resolved than the isotropic projection of 3QMAS (Figs. 4d and e). This better resolution, which was already observable in Figs. 3b and c, can be explained by the following.

In case of an infinite spinning speed, or rotor-synchronized acquisition, for each crystallite orientation, the corresponding SATRAS-ST_2 frequency is equal to (in ppm):

$$\delta_{ST2}(\theta,\varphi) = \delta_{cs} + \delta^{QIS}_{ST2} + 10^6 m_I J/\nu_o + C^4_{ST2}(\theta,\varphi) + f(\theta,\varphi)C_Q\Delta\chi/\nu_o + B^{\Delta\nu_R}_{ST2} + B^{hom}_{ST2}, \quad (1)$$

(θ,φ) polar angles describe the rotor axis orientation with respect to the quadrupolar tensor; δ_{cs} is the chemical shift; δ^{QIS}_{ST2} is the quadrupole-induced shift; J is the scalar coupling constant between spin S and another spin I with magnetic number m_I; $C^4_{ST2}(\theta,\varphi)$ is the fourth-rank term of the 2nd-order quadrupole interaction; the fifth term describes the reintroduction of the 1st-order quadrupole interaction due to $\Delta\chi$ magic-angle misset; and the last two terms represent broadenings related to spinning speed fluctuations and homogeneous interactions, respectively. The second and fourth terms of Eq. (1) can be expressed as a function of those related to the CT transition:

$$\delta_{ST2}(\theta,\varphi) = \delta_{cs} - \delta^{QIS}_{CT}/2 + 10^6 m_I J/\nu_o + C^4_{CT}(\theta,\varphi)/18 + f(\theta,\varphi)C_Q\Delta\chi/\nu_o + B^{\Delta\nu_R}_{ST2} + B^{hom}_{ST2}. \quad (2)$$

On well-crystallized powder samples and when there is no J-coupling, the first two terms lead to one isotropic resonance. This narrow line is broadened by the fourth-term, which gives rise to a 2nd-order quadrupolar CT MAS powder pattern with a reduced (by a factor of 18) frequency spread. In addition, this powder pattern is (i) convoluted by the fifth-term that corresponds to a reduced 1st-order static quadrupolar ST_2 pattern with a total frequency spread equal to $\sqrt{2}C_Q\Delta\chi(\text{rad})/6\nu_o$ ppm, and (ii) broadened by the last two terms. In contrast, under the same conditions, the powder averaged isotropic projection of MQMAS spectra corresponds to one single isotropic narrow resonance, only broadened by homogeneous interactions [15,16]:

$$\delta_{ISO}(\theta,\varphi) = \delta_{cs} - 10\delta^{QIS}_{CT}/17 + 10^6 m_I J/\nu_o + B^{hom}_{ISO}. \quad (3)$$

Therefore, if we do not take into account the homogeneous broadening, and whatever may be the sample (with or without J couplings or distribution of surroundings), isotropic projections of MQMAS spectra should be more resolved

than SATRAS-ST_2 spectra. Indeed, in this case, the latter spectra should be subject to three different types of broadenings, in contrast to MQMAS spectra which should be fully isotropic. Therefore, the much better resolution of SATRAS-ST_2 with respect 3QMAS (Figs. 4d and e), can only be explained by the homogeneous term which is important in the case of ^{93}Nb due to its 100% natural abundance. It has indeed recently been shown [20], that the homogeneous isotropic broadening (FWHM in ppm) observed in MQMAS and STMAS is equal to:

$$B_{\mathrm{ISO}}^{\mathrm{hom}} = 10^6(T_{\mathrm{CT}} + RT_{\mathrm{p}})/\pi v_{\mathrm{o}} \mid R - p \mid T_{\mathrm{CT}}T_{\mathrm{p}}, \tag{4}$$

where T_{p} and T_{CT} are the transverse homogeneous relaxation times of the pQ and the CT coherences involved during t_1 and t_2, respectively. For the case of SATRAS-ST_2, the homogeneous broadening is equal to:

$$B_{\mathrm{ST2}}^{\mathrm{hom}} = 10^6/\pi v_o T_{\mathrm{ST2}}. \tag{5}$$

Similar homogeneous relaxation times for many coherences (CT, ST_1, ST_2, DQ, 3Q...) have already been observed [20]. Assuming identical values for spin-9/2 nuclei leads to a much larger broadening of the 3QMAS, DQ-STMAS, and DQF-STMAS [8] spectra along their isotropic dimension than that observed with SATRAS-ST_2 [20]:

$$B_{\mathrm{ISO,3Q}}^{\mathrm{hom}}/B_{\mathrm{ST2}}^{\mathrm{hom}} = B_{\mathrm{ISO,DQF}}^{\mathrm{hom}}/B_{\mathrm{ST2}}^{\mathrm{hom}} = 127/17;$$
$$B_{\mathrm{ISO,DQ}}^{\mathrm{hom}}/B_{\mathrm{ST2}}^{\mathrm{hom}} = 199/17. \tag{6}$$

The homogeneous broadening along the isotropic dimension can be decreased with the 5QMAS and ST_2MAS (using ST_2 instead of ST_1 during t_1) methods, in which case we get [20]:

$$B_{\mathrm{ISO,5Q}}^{\mathrm{hom}}/B_{\mathrm{ST2}}^{\mathrm{hom}} = 131/85; \quad B_{\mathrm{ISO,ST2}}^{\mathrm{hom}}/B_{\mathrm{ST2}}^{\mathrm{hom}} = 19/17. \tag{7}$$

However, 5QMAS and ST_2MAS efficiencies and rotor-synchronized spectral-widths are very small [15,20].

In conclusion, the SATRAS-ST_2 method allows the observation in a short experimental time, of 1D spectra with highly improved resolution for spin-9/2 nuclei displaying a much better resolution than that observed on the isotropic projection of 2D 3QMAS and ST_1MAS (DQ/DQF-STMAS) methods. This enhanced resolution results from the much smaller homogeneous broadening that occurs in the SATRAS-ST_2 spectra in comparison with 3Q/ST_1-MAS spectra. It is important to note that the SATRAS-ST_2 method does not perform well when the nuclei undergo molecular motions with a frequency approximately equal to the quadrupole interaction. Indeed, in this case, the T_{ST2} relaxation times decrease significantly and the ST_2 resonances disappear [21]. The SATRAS-ST_2 method by itself is mainly interesting in case of well-crystallized samples. For samples displaying a distribution of surroundings, the advantage of SATRAS-ST_2 with respect to the isotropic projection of 3Q/ST_1-MAS methods is much less. Indeed, any distribution of chemical shift is the same, whilst that of quadrupole-induced shift is only reduced by a factor of 2. In this case, the acquisition of a 2D (MQ/ST-MAS) spectrum is preferred to analyze individually the different distributions, while the SATRAS-ST_2 method is a source of complementary information with respect to MQ/ST-MAS experiments. For 2D MQ/ST HETCOR experiments, which only use the isotropic projection of MQ/ST-MAS experiments [22], a SATRAS-ST_2 HETCOR scheme may be advantageous in terms of resolution and sensitivity. The technical requirements of the SATRAS-ST_2 method are those of STMAS (perfect magic angle and a stabilized spinning speed) [23], and a small rotor diameter is recommended to increase the RF field and the rotor synchronized spectral-width. A wide (>1 MHz) acquisition analog-filter must be used to detect the ST_2 signal, which folds back the noise into the observed spectral window [6,11]. Therefore, one of the next steps will be to enhance the S/N ratio with an optimized data treatment.

Acknowledgments

The authors thank Region Nord/Pas de Calais, Europe (FEDER), CNRS, French Minister of Science, USTL, ENSCL, and the Bruker company for funding. They would like to acknowledge Pr.L. Montagne and Drs. A. Flambard and L. Delevoye, for providing the $Na_4Nb_8P_4O_{32}$ sample and for the numerous discussions they had together. They would also like to thank Dr. S.E. Ashbrook for her help in improving largely the text.

References

[1] E.R. Andrew, A. Bradbury, R.G. Eades, Nature (London) 182 (1958) 1659.
[2] A. Samoson, E. Lipmaa, A. Pines, High-resolution solid-state NMR, averaging of second-order effect by means of a double-rotor, Mol. Phys. 65 (1988) 1013–1018.
[3] K.T. Mueller, B.Q. Sun, G.C. Chingas, J.W. Zwanziger, T. Terao, A. Pines, Dynamic-angle spinning of quadrupolar nuclei, J. Magn. Reson. 86 (1990) 470–487.
[4] L. Frydman, J.S. Harwood, Isotropic spectra of half-integer quadrupolar spins from bidimensional magic-angle-spinning NMR, J. Am. Chem. Soc. 117 (1995) 5367–5368.
[5] Z.H. Gan, Isotropic NMR spectra of half-integer quadrupolar nuclei using satellite transitions and magic-angle-spinning, J. Am. Chem. Soc. 122 (2000) 3242–3243.
[6] S.E. Ashbrook, S. Wimperis, Rotor-synchronized acquisition of quadrupolar satellite-transition NMR spectra: practical aspects and double-quantum filtration, J. Magn. Reson. 177 (2005) 36–47.
[7] A. Samoson, Satellite-transition high-resolution NMR of quadrupolar nuclei in powders, Chem. Phys. Lett. 119 (1985) 29–32.
[8] H.T. Kwak, Z.H. Gan, Double-quantum filtered STMAS, J. Magn. Reson. 164 (2003) 369–372.
[9] S. Prasad, P. Zhao, J. Huang, J.J. Fitzgerald, J.S. Shore, Niobium-93 MQMAS NMR spectroscopy study of alkali and lead niobates, Solid State Nucl. Magn. Reson. 19 (2001) 45–62.
[10] O.B. Lapina, D.F. Khabibulin, K.V. Romanenko, Z. Gan, M.G. Zuev, V.N. Krasilnikov, V.E. Federov, ^{93}Nb NMR chemical shift scale for niobia systems, Solid State Nucl. Magn. Reson. 28 (2005) 204–224.
[11] J.P. Amoureux, C. Morais, J. Trebosc, J. Rocha, C. Fernandez, I-STMAS: a new high-resolution solid-state NMR method for half-integer quadrupolar nuclei, Solid State Nucl. Magn. Reson. 23 (2003) 213–223.

[12] R. Hsu, E.N. Maslen, D.D. Boula, N. Ishizawa, Synchrotron X-ray studies of $LiNbO_3$ and $LiTaO_3$, Acta Crystallogr. B 53 (1997) 420–428.
[13] R. Kind, H. Graenicher, B. Derighetti, F. Waldner, E. Brun, Solid. State. Commun. 6 (1968) 439–440.
[14] J.P. Amoureux, C. Fernandez, S. Steuernagel, Z-filtering in MQMAS NMR, J. Magn. Reson. A123 (1996) 116–118.
[15] J.P. Amoureux, C. Fernandez, Triple, quintuple and higher order multiple quantum MAS NMR of quadrupolar nuclei, Solid State Nucl. Magn. Reson. 10 (1998) 211–223;
Solid State Nucl. Magn. Reson. 16 (2000) 339–343.
[16] J.P. Amoureux, C. Huguenard, F. Engelke, F. Taulelle, Unified representation of MQMAS and STMAS NMR of half-integer quadrupolar nuclei, Chem. Phys. Lett. 356 (2002) 497–504.
[17] D.C. Douglas, G.E. Peterson, V.J.Mc. Brierty, Reexamination of the local electric field gradients in $LiNbO_3$, Phys. Rev. B 40 (1989) 10694–10703.
[18] G. Costentin, M.M. Borel, A. Grandin, A. Leclaire, B. Raveau, Phosphate niobium bronzes and bronzoids with the MPTBp structure: $Na_4Nb_8P_4O_{32}$ and $Na_{4-x}A_xNb_7MP_4O_{32}$ fourth members of the series $A_x(PO_2)_4(NbO_3)_{2m}$, Mater. Res. Bull. 26 (1991) 1051–1057.
[19] J.P. Amoureux, L. Delevoye, S. Steuernagel, Z. Gan, S. Ganapathy, L. Montagne, Increasing the sensitivity of 2D high-resolution NMR methods applied to quadrupolar nuclei, J. Magn. Reson. 172 (2005) 268–278.
[20] J.P. Amoureux, J. Trebosc, Homogeneous broadenings in 2D solid-state NMR of half-integer quadrupolar nuclei, J. Magn. Reson. in press, doi:10.1016/j.jmr.2006.01.008.
[21] S.E. Ashbrook, S. Antonijevic, A.J. Berry, S. Wimperis, Motional broadening: an important distinction between multiple-quantum and satellite-transition MAS NMR of quadrupolar nuclei, Chem. Phys. Lett. 364 (2002) 634–642.
[22] J.W. Wiench, G. Tricot, L. Delevoye, J. Trebosc, J. Frye, L. Montagne, J.P. Amoureux, M. Pruski, SPAM-MQMAS-HETCOR: an improved method for heteronuclear spectroscopy between quadrupolar and spin-1/2 nuclei in solid-state NMR, Phys. Chem. Chem. Phys. 8 (1) (2006) 144–150.
[23] C. Huguenard, F. Taulelle, Z.H. Gan, Optimizing STMAS, J. Magn. Reson. 156 (2002) 131–137.